Resonant scattering of isobaric ^{19}Ne and ^{19}F beams on an H target

R. Coszach, Th. Delbar, W. Galster, P. Leleux, I. Licot,* E. Liénard, P. Lipnik, C. Michotte, A. Ninane, and J. Vervier
Université Catholique de Louvain, Louvain-la-Neuve, Belgium

C. R. Bain, T. Davinson, R. D. Page, A. C. Shotter, and P. J. Woods
University of Edinburgh, Edinburgh, United Kingdom

D. Baye, F. Binon, P. Descouvemont, P. Duhamel, J. Vanhorenbeeck, and M. Vincke
Université Libre de Bruxelles, Bruxelles, Belgium

P. Decrock, M. Huyse, P. Van Duppen,† and G. Vancraeynest
Katholieke Universiteit Leuven, Leuven, Belgium

F. C. Barker
Australian National University, Canberra, Australia
(Received 28 March 1994)

Resonances in ^{20}Na above the proton threshold have been studied by scattering radioactive ^{19}Ne beams off thick polyethylene targets. The isobaric ^{19}F+p scatering was also examined. The analysis of the data under different theoretical approaches is discussed. The energy, total width, spin, and parity of two resonances in ^{20}Na were assigned unambiguously. The results are compared to those obtained by indirect methods.

PACS number(s): 25.70.Bc, 27.30.+t, 95.30.Cq, 24.30.Gd

I. INTRODUCTION

The time scale of nuclear burning in hot astrophysical sites can be of the order of a few seconds or less. As a consequence, nuclear reactions involving short-lived radioactive nuclei become important, in particular radiative proton capture in the hot CNO cycle and in the rp process [1,2]. Complex networks of exotic reactions with unstable nuclei contribute to the production of stellar energy and to the nucleosynthesis of heavier elements. Some key reactions can be identified in these networks.

An important step, in the transition from the cold to the hot CNO cycles, is the radiative proton capture reaction ^{13}N$(p,\gamma)^{14}$O, which competes with the β^+ decay ^{13}N$(\beta^+)^{13}$C [$T_{1/2}(^{13}\text{N})$= 9.96 min]. The capture reaction ^{13}N$(p,\gamma)^{14}$O is dominated by a single resonance in ^{14}O (E^* = 5.15 MeV; $J^\pi = 1^-$, $T = 1$); its energy, total, and γ widths have been measured recently in Louvain-la-Neuve; the experimental methods and the results have been described in detail elsewhere [3–6]. Other measurements, direct or indirect, of this reaction have been performed and are reported in Ref. [2].

Another important step, in the transition from the hot CNO cycle to the rp process, is the ^{19}Ne$(p,\gamma)^{20}$Na reaction [$T_{1/2}(^{19}\text{Ne})$= 17.2 s]. In some environments it is a key process for the nucleosynthesis of heavier elements beyond oxygen. The sequence ^{15}O$(\alpha,\gamma)^{19}$Ne$(p,\gamma)^{20}$Na$(p,\gamma)^{21}$Mg can lead to a breakout from the hot CNO cycle [1] and may serve as a trigger for the rp process [2]. The required stellar temperatures are $T \sim 5 \times 10^8$ K, as found, e.g., in nova explosions. The radiative capture into ^{20}Na is most likely dominated by a resonance at $E_{\text{c.m.}} \sim 450$ keV, whose spin and parity as well as total and γ widths are unknown; the resonance energy is approximately known from ^{20}Ne(p,n) and ^{20}Ne$(^3\text{He},t)$ studies [7–9]. However, the total and γ widths of this resonance could be very small; current estimates range from 10^{-3} to 10^2 eV for the total width [7,10], and from 10^{-6} to 10^{-1} eV for the γ width [7,11]. Should the lower values be correct, then other resonances at slightly higher excitation energies could also be important. More recently, the β^+ decay of ^{20}Mg has been used to obtain spectroscopic information on the ^{20}Na levels of interest [12].

At Louvain-la-Neuve we are directing our efforts toward a measurement of the resonance parameters for the ^{19}Ne$(p,\gamma)^{20}$Na reaction, i.e., of the energy, total, and γ widths, spin and parity of all relevant resonances. On-line (resonant scattering) and off-line (β^+ decay and β^+-delayed α decay of ^{20}Na) techniques are being used for this purpose. We report here on measurements of resonant scattering using ^{19}Ne beams [13,14], aiming at states between 650 and 1000 keV above the ^{19}Ne+p threshold.

In this investigation one obtains information about different ^{20}Na configurations, as well as on the uncertainties introduced by models into the analysis. As the technique

*Present address: Univ. of São Paulo, São Paulo, Brazil.
†Present address: CERN, PPE-ISOLDE, Geneva, Switzerland.

we use provides the cross sections with a high accuracy, we can determine the model dependence of the resonance parameters. To this end we parameterize the theoretical cross sections [15] with three well-known techniques: an extended Breit-Wigner (BW) formula, the R-matrix method [16], and the K-matrix method [17]. Possible differences between the three approaches provide information on the theoretical uncertainty attached to the fit.

The experiments are described in Sec. II, their results are reported in Sec. III, and the latter are discussed in Sec. IV.

II. EXPERIMENT

A. Experimental technique

The ^{19}Ne and ^{19}F isobaric beams were provided by the Louvain-la-Neuve facility [13,18]. Intensities up to 10^9 particles per second (pps) on target were achieved for the radioactive beam. The incident energies were $T_b = 19.2$ and 20.5 MeV for both beams. The polyethylene targets with thicknesses of 200–600 μg/cm^2 were self-supporting foils.

In the reverse kinematics technique used here, the protons recoil into the forward hemisphere in the laboratory (lab) [backward hemisphere in the center of mass (c.m)]. Two types of charged-particle detectors were used to register the elastically scattered beam particles and the recoil ^{12}C and protons from the polyethylene target. The first detectors were passivated ion-implanted planar Si diodes (PIPS) of $\approx$ 120 μm thickness, located at discrete lab angles $\theta_{\rm lab} = 0°$, 16.3°, 27°, 32°, 37°, with an opening angle $\Delta\theta \approx 0.5°$. For the one located at 0°, the incident beam was stopped in a 3 mg/cm^2 Al foil, and the positrons produced by the stopped ^{19}Ne were deflected by a 300 G magnetic field acting over a 30 cm length; the resulting recoil proton spectra at 0° were not seriously degraded by the energy loss straggling of the protons in the Al stopper. Conventional electronics and ADCs were used in conjunction with these PIPS detectors. The second type of detector was a large area double-sided X-Y microstrip detector [19]. This detector array was covered by a retractable 3 mg/cm^2 Al foil which stopped the scattered and recoiling heavy ions. Data were obtained in a continuous angular region ($7° \leq \theta_{\rm lab} \leq 14°$). A good energy resolution, comparable to the one obtainable with a small Si diode, was achieved by using integrated electronics, developed jointly by the University of Edinburgh and the Rutherford Appleton Laboratory [20]. The preamplifier-amplifier channels were fed into octal Silena 4×10^3 channel ADCs; timing signals were derived from an ECL trigger. Some spectra were taken without the Al stopper foil and the elastically scattered heavy ions and recoil ^{12}C were rejected by the time-of-flight technique. An overall time resolution of 4 ns was sufficient for a clean separation of the protons and the heavy ions; timing signals were derived from the cyclotron RF and the detectors.

The energy calibration of the detectors was not obvious: the energy scale was calibrated first with a 3-line α source (^{239}Pu, ^{241}Am, ^{244}Cm) and a precision pulser (at the low energy end) in an on-line mode. The linearity was checked off-line with the pulser between 500 and 9000 keV; a fifth order polynomial was required to fit the integral alinearity. The resulting proton energy calibration was believed to be better than $\pm$3 keV. The first results for ^{19}Ne+p presented in Ref. [21] used this calibration. After analyzing the data obtained during the same experiment with an isobaric ^{19}F beam, it has been realized that there were serious discrepancies when well-known resonances in ^{19}F(p,p), ^{19}F$(p,p'\gamma)$, and ^{19}F(p,α) were also used for calibration purposes [22]. It appeared that an α-particle source cannot be used to calibrate in energy the proton spectrum with high precision. The response of a silicon detector to α particles and protons is nonlinear in energy [23]. The energy necessary to create an electron-hole pair in silicon depends on the particle energy and atomic number. A substantial energy defect is found for α particles as compared to protons of similar energy. Using 5.5 MeV α particles and a precision pulser, the calibrated proton spectrum in the laboratory frame is $\sim$ 70 keV too low in energy for $E_{\rm proton} \approx 3$ MeV with respect to the calibration using well-known resonances in the isobaric beam ^{19}F+p scattering. In the following we rely entirely on the isobaric ^{19}F beam for energy calibration. The ^{19}F+p resonances at $E_{\rm c.m.} = 637$, 801, 829, and 888 keV served as calibration standard. The use of an isobaric beam yields a very precise and simple procedure: isobaric beams can be selected very easily through slight adjustment to a single trimcoil, leaving all the other experimental parameters unchanged. In fact, an isobaric stable beam is always used to set up the radioactive beam. Taking into account all experimental errors other than statistical, the absolute error in the energy scale is about $\pm$6 keV in the laboratory frame. This amounts to about $\pm$2 keV in the c.m. system.

B. Data analysis

In the reverse kinematics, the heavy ion loses a considerable fraction of its initial energy in the thick $[CH_2]_n$ targets used in the present experiment; about $\frac{2}{3}$ of its energy loss is due to the carbon content of the target. Protons recoiling into the forward hemisphere (lab frame) provide a precise probe of the excitation function through the thick target [5]. Their low energy loss (about 2 orders of magnitude less than that of the heavy ions) means that this information is not seriously distorted by straggling. The energy spread of the incident beam results in a local uncertainty regarding the precise locus of the scattering process inside the target. However, as pointed out previously [4,5,14], this does not affect the precision of the measurement very much. Although polyethylene targets suffer a steady decrease in hydrogen content, there was no sign of a nonuniform loss versus target thickness at the low beam intensities used ($< 10^9$ pps), which should have lead to distortions in energy spectra taken in successive runs at a given angle. The stability of the beam energy versus time was also checked by the stability of the upper edge of the proton spectra in successive runs.

It should be stressed also that (i) the calibration procedure using only the resonant energies of the ^{19}F+p system makes the present results completely independent of the absolute value of the beam energy (both the ^{19}F and the ^{19}Ne beams) and (ii) any contamination of the ^{19}Ne beam by ^{19}F can be monitored by the presence of α particles from the strong ^{19}F$(p,\alpha)^{16}$O reaction, which are easily located in the two-dimensional spectra; such contamination was not observed. The transformation of the raw spectra into the c.m. excitation functions is given by the Jacobian and is straightforward. Figure 1 shows c.m. excitation functions for ^{19}Ne+p and ^{19}F+p resulting from a direct transformation of the raw spectra. In reverse kinematics, the following expressions are valid between the c.m. energy $E_{\text{c.m.}}$, the energy of the incident beam T_b and the measured energy T_p of the protons recoiling at a laboratory angle θ_{lab}:

$$E_{\text{c.m.}} = (A+1)^{-1} T_b, \tag{1}$$

$$\begin{aligned} T_p &= T_b \frac{4A}{(A+1)^2} \cos^2 \theta_{\text{lab}} \\ &= E_{\text{c.m.}} \frac{4A}{(A+1)} \cos^2 \theta_{\text{lab}}, \end{aligned} \tag{2}$$

where A is the mass number of the beam.

The transformation of the scattering angle and of the differential cross section to the c.m. frame is given by

$$\theta_{\text{c.m.}} = \pi - 2\theta_{\text{lab}}, \tag{3}$$

$$\frac{d\sigma}{d\Omega}(E_{\text{c.m.}}, \theta_{\text{c.m.}}) = \frac{d\sigma}{d\Omega}(E_{\text{lab}}, \theta_{\text{lab}})/4 \cos\theta_{\text{lab}}. \tag{4}$$

The proton spectra are in fact deformed slightly by two experimental effects which had been neglected in a preliminary stage of the analysis [21]; (i) the opening angle ($\Delta\theta$) of the detectors introduces an uncertainty of the laboratory energy (ΔT_p) which, from (2), is given by

$$\Delta T_p = 2T_p \tan\theta \, \Delta\theta; \tag{5}$$

(ii) the straggling of the protons in the target and in the aluminum foil stopping the heavy ions in the measurements with the 0° PIPS detector and with the X-Y detector has to be taken into account.

Instead of performing a difficult deconvolution of the raw data it was preferred to convolute the calculations (described in the next section) with a Gaussian distribution; the full width at half maximum (Δ) of this Gaussian, which incorporates the above-mentioned effects, was determined by two methods: (i) Δ was calculated using Eq. (5) and the Bohr formula for straggling and (ii) a fit was made of the ^{19}F(p,p) data with the BW formalism (see next section) convoluted with a Gaussian distribution, the resonance energies and widths being fixed and taken from the literature [22] while Δ was the only free parameter (Fig. 1). Both methods were in good agreement. Typical values of Δ at 900 keV are 8 keV for the 0° PIPS spectrum, 8.5 keV for the 10° spectrum of the X-Y detector (straggling contributing most in both cases), and 16 keV for the 37° PIPS spectrum (the ΔT_p contribution is the most important). It should be noted that resonance energies are quite insensitive to the introduction of this Gaussian distribution; the energy calibration of the ^{19}Ne+p spectra from the ^{19}F+p spectra as described in Sec. II A thus remains valid.

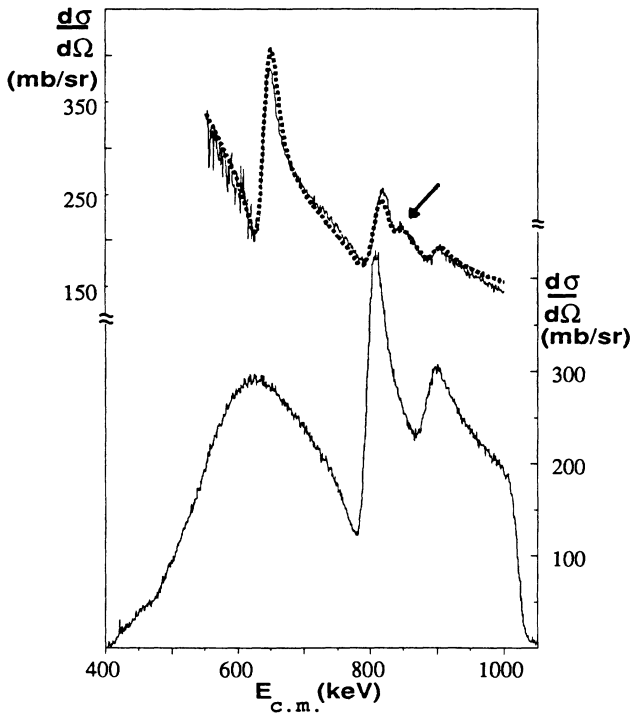

FIG. 1. Proton energy spectra at 0°, from the ^{19}F+p (top) and the ^{19}Ne+p (bottom) scattering. The ^{19}F+p spectrum fitted with a BW formula (dashed curve) has been used in the determination of the energy calibration and of the width Δ of the Gaussian distribution taking into account the experimental effects that distort the proton spectra; the arrow marks the 829 keV level which is discussed in Sec. IV.

III. RESULTS

The differential scattering cross sections have been fitted in the 106°–180° c.m. angular range and the 700-1000 keV c.m. energy range (the ^{19}Ne+p threshold is at 2199±7 keV [22] in ^{20}Na), using three different methods: the extended BW, the R-matrix, and the K-matrix formalisms.

Results obtained from fitting the data with the BW formalism are presented first. In this formalism, widths are allowed to vary with energy and the hard-sphere contribution is introduced. Cross sections are calculated as described in Ref. [15], the main contributions arising from three terms: Coulomb, resonant, and the Coulomb-resonant interference; the terms involving the hard-sphere contribution are much smaller. It was assumed, and also verified in the experimental spectra, that inelastic scattering was negligible. The penetrabilities were calculated, as in the R-matrix method, for a chan-

nel radius $R = 4.5$ fm (this point will be discussed later on), by means of the regular and irregular Coulomb wave functions. In Fig. 1, which presents a ^{19}Ne+p spectrum taken at 0°, the two prominent structures seen around $E_{\text{c.m.}} \sim 800$ and 900 keV are broad resonances. The difference between the maximum and minimum cross sections around the resonance energy reflects the statistical weight factor $\omega = (2J+1)/(2I+1)(2i+1)$ (J, I, and i are the spins of the resonance, target, and projectile, respectively). A good fit to the data over the whole angular range was obtained with an angular momentum $l = 0$ for both resonances, and $\omega = \frac{3}{4}$ and $\frac{1}{4}$, respectively, indicating J^π values of 1^+ and 0^+, respectively. The former J^π value could be reached by an $l = 0 + 2$ mixing in principle; adding an $l = 2$ component did not improve the fit. Figure 2 presents BW fits of the energy distributions at several angles. In order to estimate the importance of the experimental effects introduced in Sec. II B, pure BW calculations ($\Delta = 0$) and convoluted ones are compared in Fig. 3.

The R-matrix and K-matrix formalisms are detailed elsewhere [16,17]. Let us just recall here their main differences and their relation with the BW approximation. As long as the R-matrix parametrization is restricted to a single pole and the Thomas approximation is assumed (that the shift factor is a linear function of energy), there is no difference between this method and the extended BW formula. Note that the so-called "observed" width, and not the better known "formal" R-matrix width Γ_F, must be employed. The only difference with the BW formula comes from a nonlinearity in the energy dependence of the shift factor. The R matrix allows an introduction of further poles, either physical or simulating a background. Therefore, it offers the possibility of improving the description of off-resonance cross sections. In the limited energy range considered here, such refinements do not appear to be necessary.

The most striking feature of the K-matrix formalism is that is does not require the choice, or fit, of a channel radius. Also, no resonance shift appears in the single pole approximation. There is no distinction between formal and observed widths. With a single pole, the K-matrix expression is equivalent to a BW approximation, but with a different energy dependence of the widths, which would

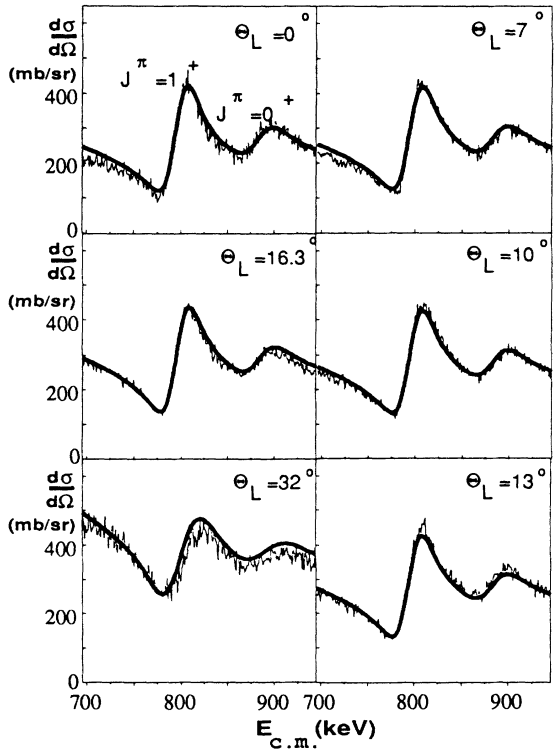

FIG. 2. Proton spectra at lab angles 0°, 16.3°, and 32° from PIPS detectors (left side) and 7°, 10°, 13° from the X-Y detector (right side), fitted with the BW formalism (solid curves). Fit with the K- or R-matrix formalism could not be distinguished from the BW curves.

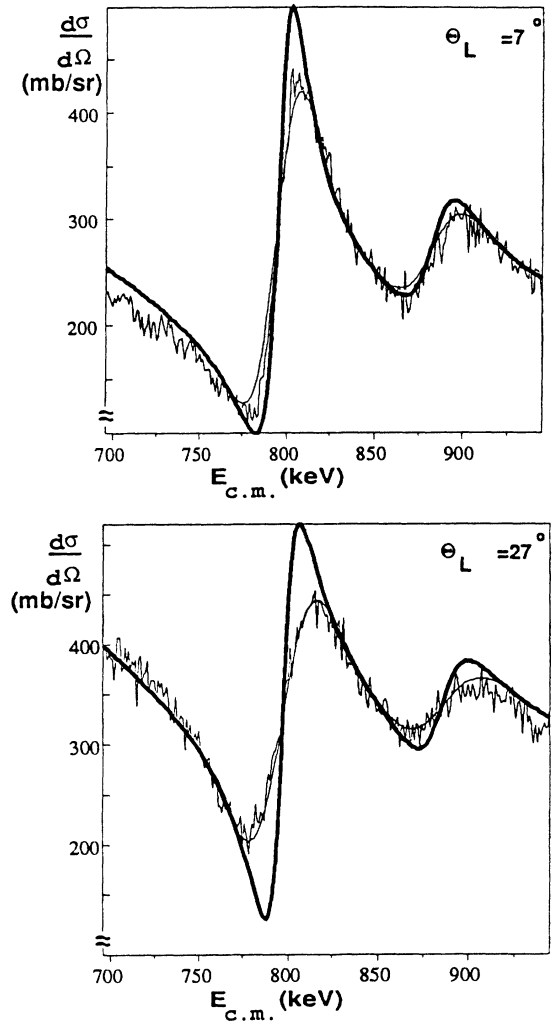

FIG. 3. Proton spectra, compared with BW, K, or R formalism (curves cannot be distinguished), without (thick curve) and with (thin curve) convolution with the experimental effects mentioned in Sec. II B: 7° spectrum measured with the X-Y detector (top) and 27° spectrum obtained with a PIPS detector (bottom).

TABLE I. Resonance energies (E_r) and widths (Γ) of the ^{20}Na resonances in the c.m. system; E_r and Γ are affected by a ± 2 keV uncertainty; γ and g are, respectively, R-matrix and K-matrix reduced widths amplitudes; Γ_F is the R-matrix formal width.

J^π	Formalism	E_r (keV)	γ or g (MeV$^{1/2}$)	Γ (keV)
1^+	BW	797		19.8
	R	797	0.92	19.8[a]
	K	797	15.6	19.8
0^+	BW	887		35.9
	R	887	1.00	35.9[b]
	K	887	15.8	35.4

[a] $\Gamma_F = 28.8$ keV ($R = 4.5$ fm).
[b] $\Gamma_F = 55.2$ keV ($R = 4.5$ fm).

correspond in the R matrix to a channel radius equal to zero. The absence of a channel radius also means that there is no obvious prescription about the treatment of nonresonant partial waves. In the R-matrix and BW approaches, a hard-sphere amplitude corresponding to the selected channel radius describes the nonresonant waves. In the K-matrix parametrization we choose the nuclear amplitude of these waves to be zero.

Fits with the R and K matrix are not shown, as they are not distinguishable from each other and from the Breit-Wigner fits. The χ^2 relative differences are in fact less than 0.5%. The results obtained with the three parametrization techniques are summarized in Table I. R-matrix and BW results depend slightly on the channel radius R: the χ^2 value improved by about 5% when decreasing R from 6 to 4.5 fm, while the Γ values changed by at most 0.5 keV; resonance energies on the other hand were not affected. Selecting the PIPS data or the X-Y detector data in the fit, we would obtain widths having a mean difference of 1.4 keV with the value of Table I, but again very stable excitation energies. In summary, the uncertainty on the resonance energies is estimated to ± 2 keV, coming entirely from the calibration (see Sec. II A), while resonance widths are affected by a ± 2 keV global uncertainty, from the different causes reported above.

IV. DISCUSSION

Let us first of all discuss Table I: as expected for single pole approximations, the three parametrizations give almost identical results. In the R matrix, the χ^2 value can be slightly improved by adding a background term in the $J^\pi = 0^+$ partial wave, but this improvement is not very significant. The χ^2 value of the K matrix is not as good as the other two, this small difference (0.5%) being attributed to the different treatment of the nonresonant waves. The 1^+ and 0^+ resonances correspond to 26 and 31 % of the Wigner limit, respectively.

Before comparing our results with previous experiments, a word of caution is needed: very narrow states would not appear in our spectra, the resonant amplitude and the Coulomb-resonance interference amplitude being proportional to Γ and $\Gamma^{1/2}$, respectively. An artificial decrease of the width of the 1^+ level was simulated in the ^{19}Ne+p spectra; Fig. 4 shows the simulated spectra incorporating the convolution with the experimental effects, for different widths. As a matter of fact, a very narrow state (< 0.5 keV) would appear only if it had a non-negligible inelastic width that would give protons of low energy, below the elastic proton pattern dominated by the Coulomb scattering. Another estimate of the limit to the small widths can be obtained when considering the ^{19}F+p spectrum (Fig. 1) in which the 829 keV resonance (located with the arrow) has a 5 keV total width and a 1 keV partial elastic width.

The positron decay of ^{20}Mg ($J^\pi = 0^+$), followed by proton emission, is a very selective process: 1^+ levels of ^{20}Na are indeed strongly favored. All experiments [12] agree on the presence of a 1^+ level at 807 ± 10 keV above the ^{19}Ne+p threshold, in excellent agreement with the present result. On the other hand, the data obtained from charge-exchange reactions, i.e., ^{20}Ne(p,n) or ^{20}Ne(^{3}He,t) [7–9], in the 600–900 keV range, are reported in Fig. 5. No clear J^π assignment has been extracted from those measurements.

The most recent charge-exchange measurement [9] has been able to deduce upper limits to the widths of the ^{20}Na excited states, by subtracting quadratically the resolution of their apparatus from the observed width of the peaks. Upper limits of 6, 10, and 16 keV were obtained for the three levels reported in Fig. 5, respectively. If the upper two levels are identified as the two levels measured in this work, then a serious discrepancy is observed concerning the width Γ. Finally it should be mentioned that shell model calculations based on a comparison with the mirror ^{20}F nucleus [7,11] lead to a 1^+ state of 19.3 or 10 keV width and a 0^+ state of 29.5 or 21 keV width in the energy range scanned in the present work; no other

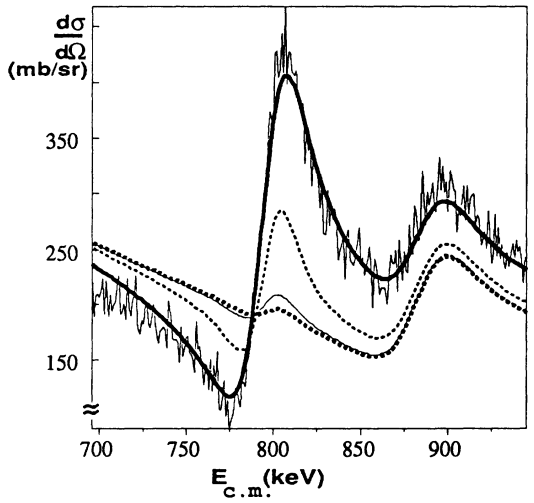

FIG. 4. Proton spectrum at 0° and calculation (thick solid line) yielding the parameters reported in Table I, among which $\Gamma(1^+) = 19.8$ keV; other curves are calculated by decreasing $\Gamma(1^+)$ to 5 keV (thin dots), 1 keV (thin solid line), and 0.5 keV (thick dots).

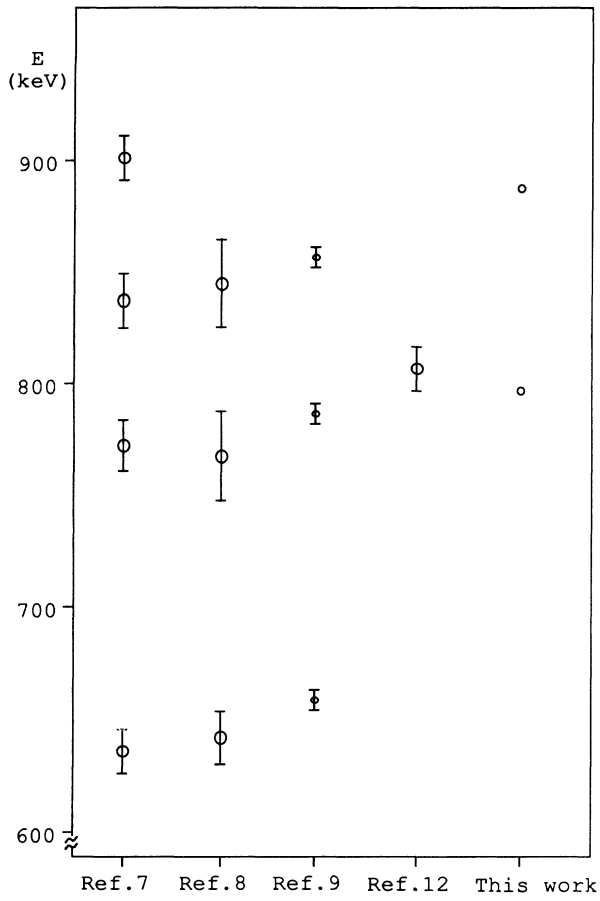

FIG. 5. Level energies (in keV above the ^{19}Ne+p threshold) obtained from different measurements: charge-exchange reactions on ^{20}Ne [7–9], β decay of ^{20}Mg [12], and present work.

states are predicted to have widths sufficiently large to be observed in the resonant scattering.

V. CONCLUSION

The energy region between 650 and 1000 keV above the ^{19}Ne+p threshold has been scanned in a single step. Two broad levels have been put in evidence, at 797 and 887 keV above threshold, or 2.996 and 3.086 MeV excitation energy in ^{20}Na, and their spin and parity have been unambiguously determined; the excitation energy and width of these levels have been deduced with high precision from fits using the BW, R-matrix, and K-matrix formalisms. Excellent agreement between the three calculations was obtained; however the narrow energy range considered in the present work could be partly responsible for that. The importance of experimental effects like the straggling of the recoil protons and the opening angle of the detectors has been emphasized.

The present results have to be complemented by other measurements, e.g., the gamma widths of the 1^+ and 0^+ levels and of low-lying levels, before significant astrophysical conclusions about the transition from the hot CNO cycle to the rp process can be deduced. Those measurements have in fact been performed recently in Louvain-la-Neuve, the data being presently analyzed.

The present method of extracting global information on unbound excited levels in a one-step measurement using the reverse kinematics and detecting recoil light particles from a thick target has been used already [4] in the ^{13}N+p case, where the resonance energy and width of an excited level in ^{14}O had been determined. While the width (around 30 keV) was in agreement with the accepted value [24], the resonance energy was off by 20 keV from the accepted value, deduced at that time from transfer or charge-exchange reactions. However, a recent measurement of the ^{12}C(^{3}He, n)^{14}O reaction [25] has confirmed the resonance energy of [4].

ACKNOWLEDGMENTS

We wish to thank the cyclotron crew for efficiently running the radioactive ion beam facility; P. Demaret for the skillful preparation of the targets; Professor H. P. Trautvetter, G. Roters, and Professor Cs. Sükösd who have contributed at different stages of the experiment. Some of us (F. Binon, P. Descouvemont, P. Leleux, G. Vancraeynest, and J. Vanhorenbeeck) acknowledge the financial support of the National Fund for Scientific Research (NFSR), Belgium. This work presents research results of the Belgian Programme on Interuniversity Poles of attraction initiated by the Belgian State, Federal Services of Scientific, Technical and Cultural Affairs.

[1] W. A. Fowler, Rev. Mod. Phys. **56**, 149 (1984); C. Rolfs and W. Rodney, *Cauldrons in the Cosmos* (University of Chicago Press, Chicago, 1988).
[2] A. Champagne and M. Wiescher, Annu. Rev. Nucl. Part. Sci. **42**, 39 (1992).
[3] P. Decrock *et al.*, Phys. Rev. Lett. **67**, 808 (1991).
[4] Th. Delbar *et al.*, Nucl. Phys. **A542**, 263 (1992).
[5] W. Galster *et al.*, Phys. Rev. C **44**, 2776 (1991).
[6] M. Benjelloun *et al.*, Nucl. Instrum. Methods Phys. Rev. A **321**, 521 (1992).
[7] L. O. Lamm *et al.*, Nucl. Phys. **A510**, 503 (1990).
[8] S. Kubono *et al.*, Astrophys. J. **344**, 460 (1989).
[9] M. S. Smith *et al.*, Nucl. Phys. **A536**, 333 (1992).
[10] P. Descouvemont and D. Baye, Nucl. Phys. **A517**, 143 (1990).
[11] B. A. Brown *et al.*, Phys. Rev. C **48**, 1456 (1993).
[12] J. Görres *et al.*, Phys. Rev. C **46**, R833 (1992); S. Kubono *et al.*, *ibid.* **46**, 361 (1992); A. Piechaczek *et al.*, in *Proceedings of the Third International Conference on Radioactive Nuclear Beams*, East Lansing, Michigan, 1993,

edited by D. J. Morrissey (Editions Frontières, Gif-sur-Yvette, 1994), p. 495.
[13] P. Decrock *et al.*, in *Proceedings of the Second International Conference on Radioactive Nuclear Beams*, Louvain-la-Neuve, 1991, edited by Th. Delbar (Adam Hilger, Bristol, 1992), p. 121.
[14] W. Galster, *ibid.* Ref. [13], p. 375.
[15] H. Feshbach, in *Nuclear Spectroscopy*, edited by F. Ajzenberg-Selove (Academic, New York, 1960), Pt. B, p. 625.
[16] A. M. Lane and R. G. Thomas, Rev. Mod. Phys. **30**, 257 (1958).
[17] J. Humblet, Phys. Rev. C **42**, 1582 (1990).
[18] D. Darquennes *et al.*, Phys. Rev. C **42**, R804 (1990).
[19] The detector was manufactured by MICRON/Sussex; the total area was 5×5 cm^2 and the X-Y pixel size was 3×3 mm^2; see [20] for details.
[20] S. L. Thomas, T. Davinson, and A. C. Shotter, Rutherford Appleton Laboratory Internal Report No. RAL-89-063; T. Davinson *et al.*, Nucl. Instrum. Methods **A288**, 245 (1990); P. J. Sellin *et al.*, *ibid.* **A311**, 217 (1991).
[21] R. Coszach *et al.*, in *Proceedings of the Third International Conference on Radioactive Nuclear Beams* [12], p. 323.
[22] F. Ajzenberg-Selove, Nucl. Phys. **A475**, 1 (1987).
[23] G. Paic *et al.*, Nucl. Instrum. Methods **188**, 119 (1981); W. N. Lennard and K. B. Winterbon, Nucl. Instrum. Methods Phys. Res. **B24/25**, 1035 (1987); D. Schardt and K. Riisager, Z. Phys. A **345**, 265 (1993).
[24] F. Ajzenberg-Selove, Nucl. Phys. **A523**, 1 (1991).
[25] P. V. Magnus, E. G. Adelberger, and A. Garcia, Phys. Rev. C **49**, R1755 (1994).